Article

Electronic Evolution of Poly(3,4-ethylenedioxythiophene) (PEDOT): From the Isolated Chain to the Pristine and Heavily Doped Crystals

Eung-Gun Kim, and Jean-Luc Bre#das

J. Am. Chem. Soc., **2008**, 130 (50), 16880-16889 • DOI: 10.1021/ja806389b • Publication Date (Web): 19 November 2008

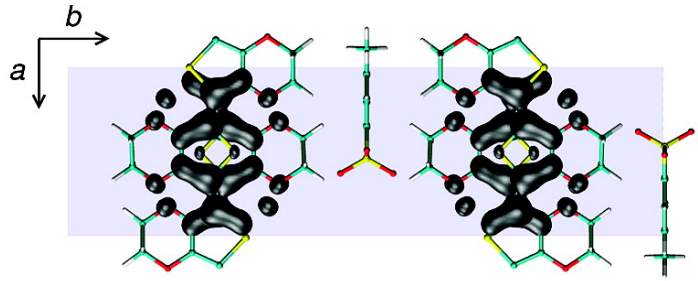

Charge Density of Metallic PEDOT:Tos at the Fermi Level

More About This Article

Additional resources and features associated with this article are available within the HTML version:

- Supporting Information
- Access to high resolution figures
- Links to articles and content related to this article
- Copyright permission to reproduce figures and/or text from this article

View the Full Text HTML

J|A|C|S
ARTICLES

Published on Web 11/19/2008

Electronic Evolution of Poly(3,4-ethylenedioxythiophene) (PEDOT): From the Isolated Chain to the Pristine and Heavily Doped Crystals

Eung-Gun Kim and Jean-Luc Brédas*

Contribution from the School of Chemistry and Biochemistry and Center for Organic Photonics and Electronics, Georgia Institute of Technology, Atlanta, Georgia 30332-0400

Received March 10, 2008; E-mail: jean-luc.bredas@chemistry.gatech.edu

Abstract: Poly(3,4-ethylenedioxythiophene) (PEDOT) is the prototypical conjugated polymer used in the doped state as the hole injection/transport layer in organic (opto)electronic devices. Numerous experimental studies have been successful only in drawing a partial microscopic picture of PEDOT due to its complex morphology, which has also hampered application of theoretical approaches. Using density functional theory methods, combined with refined structural models built upon crystallographic data of PEDOT and other substituted polythiophenes, our work seeks to establish a comprehensive understanding of the electronic and geometric structures of PEDOT, as an isolated chain and in the pristine and doped bulk phases. We find that ethylenedioxy substitution planarizes the polythiophene backbone but the experimentally observed bandgap reduction is caused mainly by a stronger destabilization of the valence band than the conduction band via donor-type substitution. The calculated crystal of pristine PEDOT has a monoclinic lamellar structure consisting of inclined π-stacks. The impact of interchain interactions on the charge carrier effective masses is greater than that of the ethylenedioxy substitution and leads to the reversal of the relative masses; the electrons are lighter than the holes in the pristine crystal. The small interchain electron effective mass is comparable to the hole effective masses found in high mobility organic crystals. Tosylic acid-doped PEDOT (PEDOT:Tos), which is receiving renewed interest as an anode material to replace indium tin oxide, is calculated to be a two-dimensional-like metal. The PEDOT:Tos crystal is found to have an embedded mirror plane in the tosylate monolayer that is sandwiched between PEDOT stacks, and thus to have twice the size of the unit cell proposed earlier. Doping is seen to remove the intrastack inclination of the PEDOT chains.

1. Introduction

Conjugated polymers and small-molecule organic materials have become omnipresent as active components in a wide range of (opto)electronic applications including light-emitting diodes (OLEDs), photovoltaic cells (OPVs), and field-effect transistors (OFETs). Also in great demand are conducting polymeric materials for use as hole injection or transport layers that are critical to improve the lifetime and efficiency of these devices.[1−3] Poly(3,4-ethylenedioxythiophene) (PEDOT; see Scheme 1a), having tunable high electrical conductivity, air stability, and transparency in the p-doped state,[4] has received most attention in this respect. For instance, when doped with a polymeric oxidant, poly(styrene sulfonic acid) (PSSH; Scheme 1b) in particular, PEDOT offers stable hole injection, low hole injection barrier, and protection of the active organic layer from reactive anode elements in OLEDs.[2,3] Electrochromic[5] and nonvolatile memory devices[6] have also been demonstrated with PSSH-doped PEDOT (PEDOT:PSS) as an active component. Increased interest in replacing inorganic anode materials with ultrahigh conductivity organic materials, together with recent advances in vapor phase polymerization, has made tosylic acid-doped PEDOT (PEDOT:Tos; Scheme 1c) another important doped form of the polymer, as demonstrated in indium tin oxide (ITO)-free OLEDs.[7]

Despite its ubiquitous presence in device applications and a wealth of data from various experimental techniques such as spectroelectrochemistry,[8−10] photoelectron spectroscopy,[11,12]

(1) Karg, S.; Scott, J. C.; Salem, J. R.; Angelopoulos, M. *Synth. Met.* **1996**, *80*, 111–117.
(2) Cao, Y.; Yu, G.; Zhang, C.; Menon, R.; Heeger, A. J. *Synth. Met.* **1997**, *87*, 171–174.
(3) Carter, S. A.; Angelopoulos, M.; Karg, S.; Brock, P. J.; Scott, J. C. *Appl. Phys. Lett.* **1997**, *70*, 2067–2069.
(4) Groenendaal, L.; Jonas, F.; Freitag, D.; Pielartzik, H.; Reynolds, J. R. *Adv. Mater. (Weinheim, Ger.)* **2000**, *12*, 481–494.
(5) Heuer, H. W.; Wehrmann, R.; Kirchmeyer, S. *Adv. Funct. Mater.* **2002**, *12*, 89–94.
(6) Möller, S.; Perlov, C.; Jackson, W.; Taussig, C.; Forrest, S. R. *Nature* **2003**, *426*, 166–169.
(7) Levermore, P. A.; Chen, L.; Wang, X.; Das, R.; Bradley, D. D. C. *Adv. Mater. (Weinheim, Ger.)* **2007**, *19*, 2379–2385.
(8) Garreau, S.; Louarn, G.; Buisson, J. P.; Froyer, G.; Lefrant, S. *Macromolecules* **1999**, *32*, 6807–6812.
(9) Łapkowski, M.; Proń, A. *Synth. Met.* **2000**, *110*, 79–83.
(10) Zykwinska, A.; Domagala, W.; Lapkowski, M. *Electrochem. Commun.* **2003**, *5*, 603–608.
(11) Greczynski, G.; Kugler, T.; Keil, M.; Osikowicz, W.; Fahlman, M.; Salaneck, W. R. *J. Electron Spectrosc. Relat. Phenom.* **2001**, *121*, 1–17.
(12) Hwang, J.; Amy, F.; Kahn, A. *Org. Electron.* **2006**, *7*, 387–396.

10.1021/ja806389b CCC: $40.75

Scheme 1. Chemical Structures of (a) Poly(3,4-ethylenedioxythiophene) (PEDOT); (b) Poly(styrene sulfonic acid) (PSSH); and (c) the Tosylate Ion (Tos)

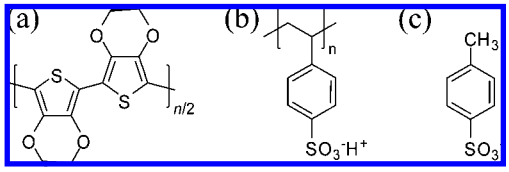

neutron reflectometry,[13] X-ray crystallography,[14] and scanning probe microscopy,[15] microscopic descriptions of the electronic and geometric structures of PEDOT in general remain far from being complete. This is due in part to the heterogeneous morphology and amorphous microstructure[14] of PEDOT:PSS, the most commonly available form of the polymer; PEDOT:PSS consists of PSSH-rich surfaces[13] and a multigrain-textured bulk (each grain with a doped region in the core and acidic PSSH in the shell).[11,15] The understanding of PEDOT is further limited by the fact that, in the case of pristine PEDOT, the majority of experimental data (both electronic and geometric) is obtained indirectly via dedoping;[8−10] only recently have developments in the polymerization of EDOT[16−18] enabled direct preparation of PEDOT in its stable pristine form, but the experimental data are limited. Theoretical calculations on *isolated* EDOT oligomers[19−22] and PEDOT[23] have provided additional information on both the pristine[19,21,23] and the doped state;[20] however, even simple questions, for instance, regarding the impact of ethylenedioxy substitution on single-chain properties such as bandgap and intrachain electronic coupling, do not seem to have definite answers, not to mention those relevant to the intricate interplay of intra- and interchain interactions.

In the present work, we use density functional theory (DFT) methods to seek to provide a consistent, three-dimensional model for the electronic and geometric structures of PEDOT. We start from a single isolated thiophene (T) monomer, the fundamental building block of the polymer, then substitute it with the ethylenedioxy group, introduce chain connectivity and interchain interactions, and finally add dopants. Tos, with which PEDOT forms a well-defined crystal,[24] is used as the dopant ion. The crystal structures of pristine and doped PEDOT are built upon X-ray crystallographic data of PEDOT and polythiophenes (PTs) with different substituents and with different dopants, and are refined with the DFT calculations. The three-dimensional electronic band structure is calculated and charge transport is discussed within the effective mass approximation. Finally, a two-phase model, consisting of PEDOT:Tos as the bulk (Tos can be viewed as the monomeric counterpart of PSS) and PSSH as the surface, is presented for PEDOT:PSS.

2. Methodology

For calculations on isolated molecules and isolated chains, each molecule/chain was placed in an orthorhombic cell padded with a vacuum spacing of about 7 Å in all three (two for the chains) directions. The Hockney Poisson solver[25] was used to treat long-range Coulombic interactions in the case of the monomers and oligomers. Two stereoisomers in three dyad conformations (meso in *TG*+, and racemic in *TT* and *G*+*G*+, where *T* is for trans and *G* for gauche) were generated for a dimer of *p*-styrene sulfonic acid (DSSH) with both ends terminated by a methyl group to represent the local structure of PSSH. *k*-Point sampling was used for periodic systems with Monkhorst−Pack meshes[26] of 6 × 1 × 1, 6 × 4 × 6, and 6 × 2 × 8 for the isolated chains, the PEDOT crystal, and the PEDOT:Tos crystal, respectively.

The DIIS[27] and L-BFGS[28] methods were used for optimization of wavefunction and geometry, respectively, of the isolated molecules and PEDOT crystal. The band structure of the PEDOT crystal was calculated in a non-self-consistent manner from the optimized electron density with an iterative Lanczos diagonalization.[29]

In the case of the PEDOT:Tos crystal, the wavefunction optimization was performed with the Davidson diagonalization method[30] along with the Methfessel−Paxton scheme[31] for efficient Brillouin zone integration in metals. The standard BFGS method was used for geometry optimization. The band structure was calculated with the standard Davidson diagonalization. The calculation of the density of states (DOS) was performed, also non-self-consistently, with the tetrahedron method[32] for Brillouin zone integration at the special *k*-points shifted by half the grid sizes.

Calculations were carried out within the generalized gradient approximation (GGA) by using the BLYP exchange−correlation functionals. For all systems except for the PEDOT:Tos crystal, norm-conserving numerical pseudopotentials generated with the procedure of Troullier and Martins[33] were used for C, S, and O, and a local analytic pseudopotential for H, with a plane-wave energy cutoff of 70 Ry for the wavefunction (280 Ry for the electron density); calculations were carried out using the CPMD (Car−Parrinello Molecular Dynamics) code.[34] For PEDOT:Tos, Vanderbilt ultrasoft pseudopotentials[35] were used with an energy cutoff of 25 Ry for the wavefunction (200 Ry for the electron density); calculations were performed with the PWscf (Plane-Wave Self-Consistent Field) code.[36]

(13) Jukes, P. C.; Martin, S. J.; Higgins, A. M.; Geoghegan, M.; Jones, R. A. L.; Langridge, S.; Wehrum, A.; Kirchmeyer, S. *Adv. Mater. (Weinheim, Ger.)* **2004**, *16*, 807–811.
(14) Breiby, D. W.; Samuelsen, E. J.; Groenendaal, L.; Struth, B. *J. Polym. Sci., Polym. Phys. Ed.* **2003**, *41*, 945–952.
(15) Nardes, A. M.; Kemerink, M.; Janssen, R. A. J.; Bastiaansen, J. A. M.; Kiggen, N. M. M.; Langeveld, B. M. W.; van Breemen, A. J. J. M.; de Kok, M. M. *Adv. Mater. (Weinheim, Ger.)* **2007**, *19*, 1196–1200.
(16) Tran-Van, F.; Garreau, S.; Louarn, G.; Froyer, G.; Chevrot, C. *J. Mater. Chem.* **2001**, *11*, 1378–1382.
(17) Yamamoto, T.; Shiraishi, K.; Abla, M.; Yamaguchi, I.; Groenendaal, L. *Polymer* **2002**, *43*, 711–719.
(18) Reuter, K.; Kirchmeyer, S. U.S. Patent 6,756,473, 2004.
(19) Dkhissi, A.; Louwet, F.; Groenendaal, L.; Beljonne, D.; Lazzaroni, R.; Brédas, J. L. *Chem. Phys. Lett.* **2002**, *359*, 466–472.
(20) Dkhissi, A.; Beljonne, D.; Lazzaroni, R.; Louwet, F.; Groenendaal, L.; Brédas, J. L. *Int. J. Quantum Chem.* **2003**, *91*, 517–523.
(21) Osikowicz, W.; Denier van der Gon, A. W.; Crispin, X.; de Jong, M. P.; Friedlein, R.; Groenendaal, L.; Fahlman, M.; Beljonne, D.; Lazzaroni, R.; Salaneck, W. R. *J. Chem. Phys.* **2003**, *119*, 10415–10420.
(22) Alemán, C.; Casanovas, J. *J. Phys. Chem. A* **2004**, *108*, 1440–1447.
(23) Brocks, G. *J. Phys. Chem.* **1996**, *100*, 17327–17333.
(24) Aasmundtveit, K. E.; Samuelsen, E. J.; Pettersson, L. A. A.; Inganäs, O.; Johansson, T.; Feidenhans'l, R. *Synth. Met.* **1999**, *101*, 561–564.
(25) Hockney, R. W. *Methods Comput. Phys.* **1970**, *9*, 135–211.
(26) Monkhorst, H. J.; Pack, J. D. *Phys. Rev. B* **1976**, *13*, 5188–5192.
(27) Hutter, J.; Lüthi, H. P.; Parrinello, M. *Comput. Mater. Sci.* **1994**, *2*, 244–248.
(28) Billeter, S. R.; Curioni, A.; Andreoni, W. *Comput. Mater. Sci.* **2003**, *27*, 437–445.
(29) Pollard, W. T.; Friesner, R. A. *J. Chem. Phys.* **1993**, *99*, 6742–6750.
(30) Davidson, E. R. *J. Comput. Phys.* **1975**, *17*, 87–94.
(31) Methfessel, M.; Paxton, A. T. *Phys. Rev. B* **1989**, *40*, 3616–3621.
(32) Blöchl, P. E.; Jepsen, O.; Andersen, O. K. *Phys. Rev. B* **1994**, *49*, 16223–16233.
(33) Troullier, N.; Martins, J. L. *Phys. Rev. B* **1991**, *43*, 1993–2006.
(34) CPMD, 3.9.2; IBM Corp and Max-Planck-Institut für Festkörperforschung Stuttgart: 2005.
(35) Vanderbilt, D. *Phys. Rev. B* **1990**, *41*, 7892–7895.
(36) PWscf, 3.2.3; DEMOCRITOS National Simulation Center of INFM: 2007.

The inverse effective mass tensor for the three-dimensional crystal, m_{ji}^{-1}, is defined as[37]

$$m_{ji}^{-1} = \frac{1}{\hbar^2}\frac{\partial^2 \varepsilon}{\partial k_j \partial k_i} \quad (1)$$

where ε denotes the band energy, $\hbar$ the Planck constant, k the electron momentum, and subscripts i and j the Cartesian coordinates in reciprocal space. Subsequent diagonalization of m_{ji}^{-1} provides the principal components and their orientations. The inverse effective mass tensor was calculated using Sperling's centered difference method with dk = 0.0032 (2π/Å).

The simulation of UPS spectra was performed according to the standard procedure[38,39] that has been shown to account effectively for solid state polarization and disorder. The calculated DOS was convolved with a Gaussian function of fwhm (full width at half maximum) = 0.8 eV; the energy levels were rescaled by an expansion factor of 1.2; and a shift along the energy axis was then applied to the entire spectrum to match against experimental peaks. Assuming that PSSH follows the tacticity and conformational statistics of atactic polystyrene (meso = 0.46),[40] we summed three simulated spectra with statistical weights based on 2,4-diphenylpentane (*TG*+(meso) = 0.99, *TT*(racemic) = 0.78, and *G*+*G*+(racemic) = 0.21) to obtain the spectrum of PSSH. The same procedure was applied to PEDOT:Tos.

3. Results and Discussion

3.1. Isolated Chain. Isolated chains of PEDOT and PT were modeled by crystals with one-dimensional periodicity, consisting of two monomeric units in the unit cell. The unit cell length was optimized by performing geometry optimization with varying cell dimension. Isolated monomers and oligomers (EDOT*n* and T*n*, where $n = 2-4$) of EDOT and T were also calculated.

The C−C bond of the ethylenedioxy group can assume either the *G*+ or *G*− conformation. The dyad conformation in the unit cell of PEDOT was set to *G*+*G*− (or *G*−*G*+) according to the experimental crystal structures of EDOT2[41] and EDOT3 end-capped with alkyl groups[42] (see Scheme 1a for the conformations of the ethylenedioxy groups).

3.1.1. Effect of Ethylenedioxy Substitution on the Geometry. Figure 1, top panel shows the evolution of the backbone bond lengths with increasing chain length (see also Table 1 for other geometric parameters). The C−C bonds, both intra- and inter-ring, shorten whereas the C=C bonds lengthen; the changes in the latter are less pronounced. Similar behavior is seen for the unsubstituted thiophene series (results not shown). At infinite chain length, PEDOT remains aromatic-like (its bond length alternation remains finite and, in our convention, positive), as does PT; our conclusion is consistent with that of a previous theoretical study of EDOT oligomers,[19] in which the energy per monomeric unit was estimated and compared to that of the quinoid-like form.

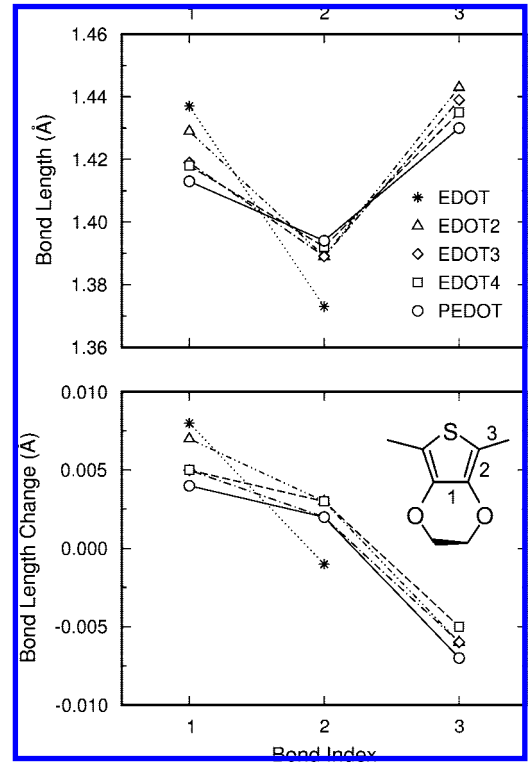

Figure 1. Effects of chain length and ethylenedioxy substitution on the bond length alternation in isolated EDOT homologs. The bond length change in the bottom panel is with respect to the unsubstituted thiophene counterparts. All values for the oligomers are from the innermost units.

Table 1. Geometric Parameters of the EDOT Monomeric Unit[a] at Different Chain Lengths

distance (Å)	EDOT	EDOT2	EDOT3	EDOT4	PEDOT	PT
S−C	1.737	1.768	1.768	1.767	1.772	1.763
O···S[b]		2.970	2.933	2.954	2.952	
end-to-end[c]			3.961	3.958	3.963	3.935

[a] All values for the oligomers are from the innermost units. [b] We note that the sum of the van der Waals radii for O and S amounts to ~3.32 Å. [c] The monomeric end-to-end distance is defined as the distance between the midpoints of two consecutive inter-ring bonds (=*a*/2 for the polymers).

The effect of the ethylenedioxy substitution on the backbone geometry may be best monitored by changes in bond length upon substitution (see Figure 1, bottom panel). The intra-ring C−C and C=C bonds both lengthen whereas the inter-ring C−C bond shortens in all cases with the exception of the monomer, for which the C=C bond slightly shortens. The lengthening of the intra-ring C−C bond is a direct consequence of interactions with the O atoms. The different behavior of EDOT is due to a very different wavefunction pattern of its highest occupied molecular orbital (HOMO), as will be discussed later.

Crystallographic evidence[41,42] on EDOT oligomers strongly suggests that there occur O···S interactions leading to planarization of the thiophene backbone; without ethylenedioxy substitution, a fully coplanar conformation is not the energy minimum, as confirmed also by high-level theoretical calculations on isolated T2.[43,44] It should be noted that all of our

(37) Seeger, K. *Semiconductor Physics: An Introduction*, 9th ed.; Springer-Verlag: Berlin, 2004.
(38) Cornil, J.; Vanderdonckt, S.; Lazzaroni, R.; dos Santos, D. A.; Thys, G.; Geise, H. J.; Yu, L.-M.; Szablewski, M.; Bloor, D.; Lögdlund, M.; Salaneck, W. R.; Gruhn, N. E.; Lichtenberger, D. L.; Lee, P. A.; Armstrong, N. R.; Brédas, J. L. *Chem. Mater.* **1999**, *11*, 2436–2443.
(39) Hwang, J.; Kim, E.-G.; Liu, J.; Brédas, J.-L.; Duggal, A.; Kahn, A. *J. Phys. Chem. C* **2007**, *111*, 1378–1384.
(40) Sato, H.; Tanaka, Y.; Hatada, K. *Makromol. Chem.−Rapid Commun.* **1982**, *3*, 181–185.
(41) Raimundo, J.-M.; Blanchard, P.; Frère, P.; Mercier, N.; Ledoux-Rak, I.; Hierle, R.; Roncali, J. *Tetrahedron Lett.* **2001**, *42*, 1507–1510.
(42) Turbiez, M.; Frère, P.; Roncali, J. *J. Org. Chem.* **2003**, *68*, 5357–5360.
(43) Ortí, E.; Viruela, P. M.; Sánchez-Marín, J.; Tomás, F. *J. Phys. Chem.* **1995**, *99*, 4955–4963.
(44) Alemán, C.; Domingo, V. M.; Fajarí, L.; Juliá, L.; Karpfen, A. *J. Org. Chem.* **1998**, *63*, 1041–1048.

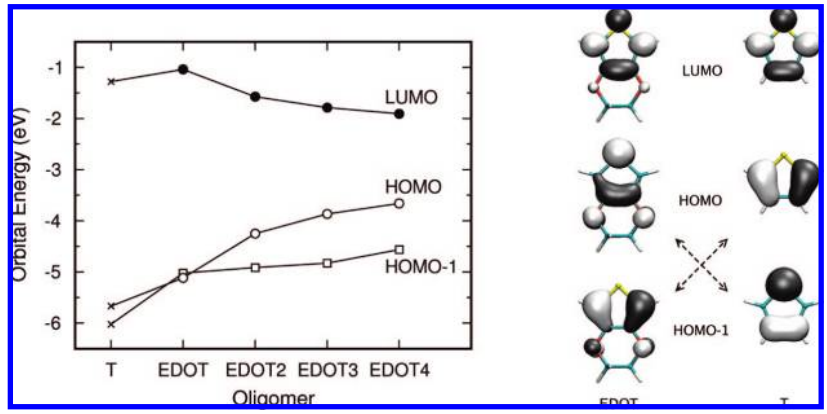

Figure 2. Evolution of the frontier molecular orbital energies with chain length in EDOT homologs. Values for T are also shown for comparison. The connecting lines for HOMO and HOMO−1 were drawn to follow the same wavefunction pattern with varying chain length. To the right of the plot are the wavefunction patterns in EDOT and T, with the dashed lines illustrating the reversal of the HOMO/HOMO−1 wavefunctions in going from T to EDOT.

comparisons to the thiophene counterparts are made in relation to the coplanar conformations, so that only the effects of substitution can be assessed without those of planarization (which alone can affect both the geometric and electronic structures); experimentally, it is also the case when PEDOT is compared to PT because nearly all thiophene homologs in the solid state are found to adopt a coplanar conformation.[45−49]

The strength of the nonbonded O···S interaction, E(O···S), can be estimated from the following expression:

$$E(\mathrm{O}\cdots\mathrm{S}) = \frac{1}{2}[(E^{90}_{\mathrm{PEDOT}} - E^{180}_{\mathrm{PEDOT}}) - (E^{90}_{\mathrm{PT}} - E^{180}_{\mathrm{PT}})] \qquad (2)$$

Here the superscripts 90 and 180 denote the inter-ring torsions at which the total energy of the system, E, is calculated and the 1/2 factor reflects that there are two O···S pairs being separated upon rotation of an inter-ring C−C bond (note that a 90° rotation translates into a displacement from ∼0.4 Å shorter to ∼0.7 Å longer than the sum of their van der Waals radii). Previous calculations have shown[22,44] that although the shape of the DFT torsional potential energy surface is very close to that of an MP2 result, the torsional energy barrier is not. Therefore, we used the MP2/6-31G(d) results[50] for EDOT2[22] and T2[44] to estimate E(O···S), which is on the order of 1.2 kcal/mol (or ∼2.4 kcal/mol to twist a pair of adjacent EDOT rings out of the plane). Whereas these attractive interactions pull adjacent EDOT units toward each other and shorten the inter-ring C−C bond (Figure 1, bottom panel), it is interesting to note that, overall, PEDOT has a larger unit cell length than PT (see Table 1).

Planarization through nonbonded intrachain interactions is also found in 2,5-alkoxy-substituted poly(*p*-phenylene vinylene)s, via O···H hydrogen bonding.[51,52] Antibonding interactions of the alkoxy group with the phenylene ring destabilize the HOMO, the same effect as that found in PEDOT, as discussed below.

3.1.2. Effect of Ethylenedioxy Substitution on the Electronic Structure. Another effect of the donor-type ethylenedioxy substitution is the destabilization of both the HOMO and LUMO (lowest unoccupied molecular orbital) levels.[53] It can be simply illustrated by comparison of the two monomers, EDOT and T, as shown in Figure 2. The antibonding interactions between the O and backbone C atoms push up the orbital energy levels to different extents, in the order HOMO−1 > HOMO > LUMO (the different degrees of destabilization may be roughly visualized by inspection of the charge density on the O atoms in the wavefunction patterns in Figure 2, right panel). In the case of HOMO−1, the antibonding interactions are so large that its stability with respect to HOMO becomes reversed in going from T to EDOT; the relative stability is recovered in the dimer and larger oligomers as a result of inter-ring interactions (see the line crossings in Figure 2, left panel). The more pronounced destabilization of the HOMO than of the LUMO results in a reduction of the bandgap[53] and is responsible for most of the bandgap difference between the polymeric counterparts seen experimentally[16,54] and in our calculated band structures reported in Figure 3.

As can be expected from the evolution of the electronic structure in the monomer and oligomers, the general shape of the isolated-chain band structure of PEDOT is very similar to that of PT; in particular, the upper part of the valence band consists of two dispersive (b and e in Figure 3) and two flat (c and d) subbands, as thoroughly discussed in earlier work on PT.[55] Briefly, the two strongly dispersive subbands in PEDOT originate from the monomer HOMO−1s (HOMOs in the case of PT) interacting via bonding and antibonding interactions along the chain backbone (compare HOMO−1 in Figure 2 with the antibonding b in Figure 3). On the other hand, the other two subbands from the monomer HOMOs (HOMO−1s for PT)

(45) Brückner, S.; Porzio, W. *Makromol. Chem.* **1988**, *189*, 961–967.
(46) Tashiro, K.; Ono, K.; Minagawa, Y.; Kobayashi, M.; Kawai, T.; Yoshino, K. *J. Polym. Sci., Polym. Phys. Ed.* **1991**, *29*, 1223–1233.
(47) Prosa, T. J.; Winokur, M. J.; Moulton, J.; Smith, P.; Heeger, A. J. *Macromolecules* **1992**, *25*, 4364–4372.
(48) Meille, S. V.; Romita, V.; Caronna, T.; Lovinger, A. J.; Catellani, M.; Belobrzeckaja, L. *Macromolecules* **1997**, *30*, 7898–7905.
(49) Fichou, D. *J. Mater. Chem.* **2000**, *10*, 571–588.
(50) MP2 calculations are known to be sensitive to the size of the basis set due to strong effects of the basis set superposition error (BSSE) on electron correlation. This BSSE in binding energy is large even for a very large basis set (Sinnokrot, M. O.; Valeev, E. F.; Sherrill, C. D. *J. Am. Chem. Soc.* **2002**, *124*, 10887−10893), and cannot be easily corrected in the case of intramolecular binding. Interestingly, however, MP2/6-31G(d) gives intermolecular binding energies of benzene dimers in reasonable agreement with those obtained at MP2/6-311G(2d,2p) with corrections for BSSE (Jaffe, R. L.; Smith, G. D. *J. Chem. Phys.* **1996**, *105*, 2780−2788).
(51) Lhost, O.; Brédas, J.-L. *J. Chem. Phys.* **1992**, *96*, 5279–5288.
(52) Fahlman, M.; Lögdlund, M.; Stafström, S.; Salaneck, W. R.; Friend, R. H.; Burn, P. L.; Holmes, A. B.; Kaeriyama, K.; Sonoda, Y.; Lhost, O.; Meyers, F.; Brédas, J. L. *Macromolecules* **1995**, *28*, 1959–1965.
(53) Brédas, J.-L.; Heeger, A. J. *Chem. Phys. Lett.* **1994**, *217*, 507–512.
(54) Kobayashi, M.; Chen, J.; Chung, T.-C.; Moraes, F.; Heeger, A. J.; Wudl, F. *Synth. Met.* **1984**, *9*, 77–86.
(55) Brédas, J. L.; Elsenbaumer, R. L.; Chance, R. R.; Silbey, R. *J. Chem. Phys.* **1983**, *78*, 5656–5662.

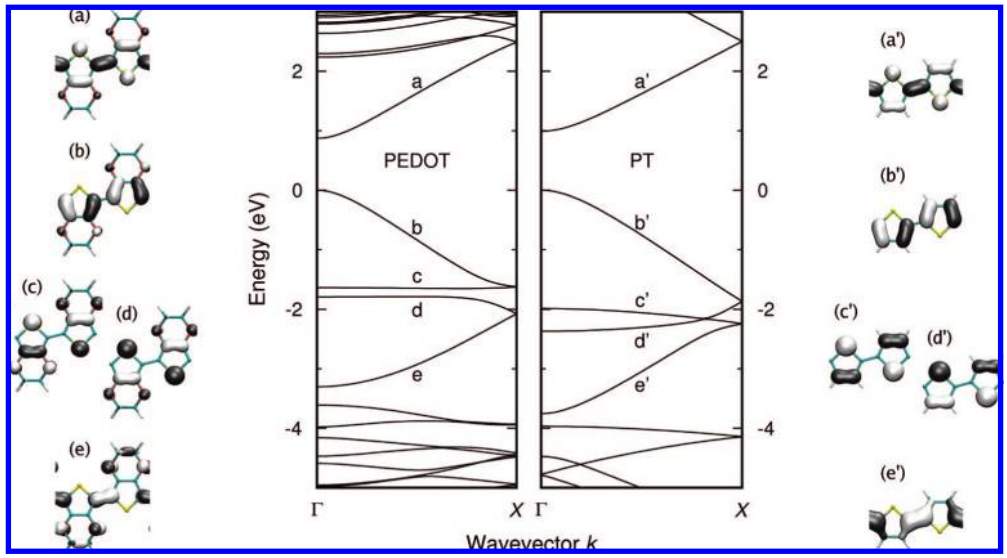

Figure 3. Comparison of the electronic band structures of the isolated PEDOT and PT chains. To both sides of the center panel are the wavefunction patterns of the crystalline orbitals of the labeled subbands at the Γ-point (the left panel for PEDOT and the right for PT). The energy levels are shifted such that the valence band edges align with zero. For the points of high symmetry in the first Brillouin zone, for the sake of consistency, the same labeling scheme as for the three-dimensional orthorhombic crystals is used here for the one-dimensional isolated chain ($X = (0.5, 0, 0)$ in crystallographic coordinates and the chain backbone is oriented along the *a*-axis).

Table 2. Calculated Values of the Bandgap, E_g, Bandwidth, *W*, and Effective Mass, *m*, of PEDOT

	isolated chain[a]	pristine crystal[b]
E_g (eV)[c]	0.87 (0.99)	0.37
W for the valence band (eV)[d]	3.30 (3.76)	3.65
m/m_0 for the hole[e]	0.093 (0.12)	0.13 (*a*), 4.8 (*c*)
m/m_0 for the electron	0.099 (0.14)	0.078 (*a*), 1.6 (*c*)

[a] Values in parentheses are for PT. [b] Values in parentheses are the crystal axes parallel to the respective principal axes of the inverse effective mass tensor. [c] Unscaled values. [d] Values represent the full widths of the four and eight topmost subbands for the isolated chains and the crystal, respectively. [e] m_0 is the free electron mass at rest.

are nearly flat due to the fact that the wavefunction presents nodes on the carbon atoms involved in the inter-ring bonds (compare HOMO in Figure 2 with c or d in Figure 3).

The Kohn−Sham one-electron bandgap from the band structure is smaller for PEDOT than for PT (see also Table 2). Although in general no direct comparison to experiment can be made due to a discontinuity in the exchange−correlation potential upon removal/addition of an electron,[56] the DFT values have been successfully correlated with experimental optical transitions in a variety of conjugated polymers by introduction of a common empirical scaling factor.[57] The calculated bandgaps, when scaled by 200%, are in line with the experimental values (the onset/peak maximum positions in the solid-state optical absorption spectra are 1.8/2.4 eV for PEDOT[16] and 2.0/2.7 eV for PT[54]). Comparison of the band structure also indicates that the valence band of PEDOT (considering subbands b to e) is wide (3.3 eV) but somewhat narrower (by 0.46 eV) than that of PT. This is due to the reduced charge density on the backbone C atoms as a result of delocalization onto the O atoms, which in turn weakens the interactions among monomeric units in the backbone (see the wavefunction patterns in Figures 2 and 3).

In the case of wide bands (or at low temperature), where only the states around the band edges are populated, the description of many properties including charge transport can be simplified by using the effective mass approximation. The concept of effective mass derives from the simple idea that an electron in a crystal can be treated as a free particle but with an effective mass that accounts for the effect of the periodic crystal potential.[37] The effective mass, *m*, for the system with one-dimensional periodicity (see the Methodology section for the three-dimensional case) is defined as

$$m^{-1} = \frac{1}{\hbar^2}\frac{d^2\varepsilon}{dk^2} \tag{3}$$

where ε denotes the band energy, $\hbar$ the Planck constant, and *k* the electron momentum.

The hole effective mass along the chain axis, calculated at the valence band edge, is smaller in PEDOT than in PT, as shown in Table 2 (note that the opposite would be expected from a simplistic comparison of the full bandwidths). The electron also has a smaller effective mass in PEDOT (calculated at the conduction band edge) than in PT. The hole is slightly lighter than the electron in both PEDOT and PT.

3.2. Pristine Crystal. In their more commonly observed polymorph (form I),[48,58] the much-studied poly(3-alkyl thiophene)s (or P3ATs) pack in an orthorhombic lattice with a lamellar structure; in each layer, individual chain backbones stack, shifted along the chain axis over another by one thiophene ring.[46−48] The orthorhombic lamellar structure of P3ATs is not perturbed by varying the alkyl side group length C_n ($n = 4-16$)[48] (note that unsubstituted PT forms a herringbone structure in the orthorhombic lattice[45]) or by moderate doping with small molecules.[59] These experimental observations, along with the fact that the thiophene chain backbones in both PEDOT[24] and P3ATs[59] share the same packing in the doped state, strongly suggest that pristine PEDOT could also adopt a lamellar structure in an orthorhombic unit cell (see Figure 4).

(56) Godby, R. W.; Schlüter, M.; Sham, L. J. *Phys. Rev. B* **1988**, *37*, 10159–10175.
(57) Brocks, G.; Kelly, P. J.; Car, R. *Synth. Met.* **1993**, *55−57*, 4243–4248.
(58) Prosa, T. J.; Winokur, M. J.; McCullough, R. D. *Macromolecules* **1996**, *29*, 3654–3656.
(59) Prosa, T. J.; Winokur, M. J.; Moulton, J.; Smith, P.; Heeger, A. J. *Phys. Rev. B* **1995**, *51*, 159–168.

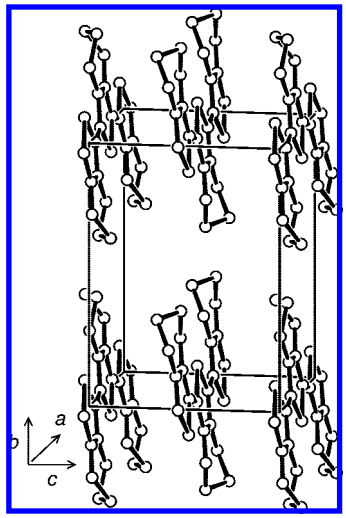

Figure 4. Calculated structure of the pristine PEDOT crystal. The orthorhombic unit cell ($a/b/c$ = 7.935/10.52/7.6 Å) contains two chains, each with two EDOT units; a was optimized in this work whereas b and c were taken from experiment (see text for details). For clarity, the hydrogen atoms are not shown. The monoclinic representation of the calculated crystal structure has lattice parameters a = 12.978 Å, b = 7.935 Å, c = 7.6 Å, and β = 125.85°.

The unit cell length c along the stacking direction of P3ATs, which is invariant with side chain length,[47,48,58] was taken to construct a model for the PEDOT crystal (c = 7.6 Å). The cell length a along the backbone axis was obtained by calculating the potential energy surface, as done for the isolated chain. The interstack distance or cell length b was taken from (rather crude) X-ray crystallographic data[16] on pristine PEDOT (b = 10.52 Å). Although b is the least important cell parameter in understanding the effect of intermolecular interactions on the electronic structure in the pristine crystal, our fully optimized crystal structure ensured that this value is reasonable (the closest interlayer H···H distances corresponding to the sum of their van der Waals radii).

3.2.1. Chain Backbone Rotation. Within the structural model of an orthorhombic lamellar structure, two internal geometric parameters are yet to be determined: (i) the relative orientations of the ethylene bridges between neighboring chains and (ii) the rotation of the chains around their backbone axis. With two chains in the unit cell, each with the ethylene bridges in the $G+G-$ conformation, there are two different ways to stack the chains along the c-axis. The stacking sequence with the ethylene bridges forming a herringbone pattern (Figure 5, top panel) is 0.6 kcal/mol per unit cell more stable than the "stack-and-slip" sequence; in the less favorable stack-and-slip configuration, adjacent chains have the ethylene bridges oriented in the same direction. We note that there are deep "hollow" sites (bounded by four ethylene groups and one underlying sulfur atom) on each surface of the PEDOT layer.

Chain backbone rotation has been noted experimentally in the case of P3ATs; the rotation angle, φ, defined by the angle between the chain backbone plane and the (001) crystal plane, increases (5−13°) with side chain length.[47] In order to locate the energy minimum for the PEDOT crystal, we rotated (from 0° to 15° by increments of 5°) both chains of the unit cell before turning on the full geometry optimization at the fixed lattice constants. The two chains were rotated simultaneously in the same sense.

The energy minimum crystal structure thus found has a rotation angle of 8.9° (stacking distance = 3.754 Å) (see Figure 5, bottom panel); rotation of the backbone lowers the total energy by 1.4 kcal/mol per unit cell with respect to the φ = 0° crystal. The inclining ethylenedioxy groups toward the adjacent chains are well accommodated within the hollows (see Figure 5). As a result of the rotation, an EDOT unit is no longer symmetric along the backbone. The pristine PEDOT crystal, with the detailed molecular structure from our calculations, can be better represented by a monoclinic lattice (space group $P2/c$; see also the caption of Figure 4).

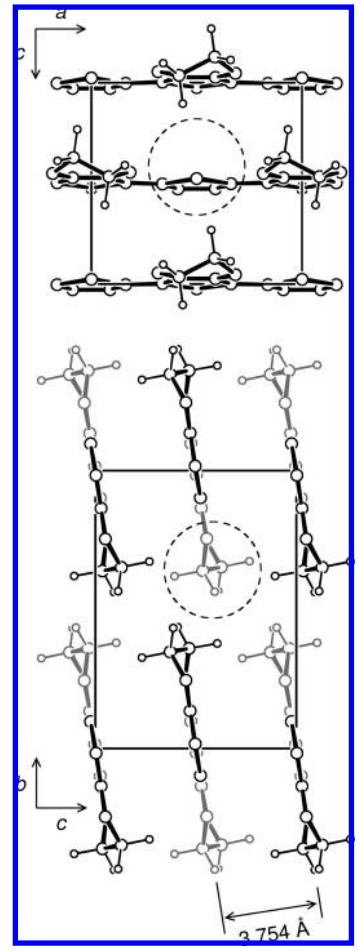

Figure 5. Interchain stack sequence (top) and chain backbone rotation (bottom) in the calculated pristine PEDOT crystal. The stack sequence, with respect to the ethylene bridge orientation, is in the herringbone configuration (the bottom half of the unit cell and the ethylenedioxy groups facing down are not drawn for clarity). Dashed circles denote a representative hollow site on each surface of the PEDOT layer.

The intrachain bond lengths remain nearly unaffected by interchain interactions (<0.002 Å). The O···S distance is lengthened by 0.007 Å, which is reflected in the slightly increased a value with respect to the isolated chain (by ∼0.01 Å).

Our procedure for determining the conformation of the ethylenedioxy group and the rotation of the chain backbone may warrant some justification. In spite of the inability of conventional DFT methods to describe van der Waals interactions,[60] numerous studies have shown that constraining the lattice constants to experimental values effectively compensates the missing attractive interactions. As a result, such DFT calculations have been found to accurately reproduce not only the

(60) Zhao, Y.; Truhlar, D. G. *J. Chem. Theory Comput.* **2005**, *1*, 415–432.

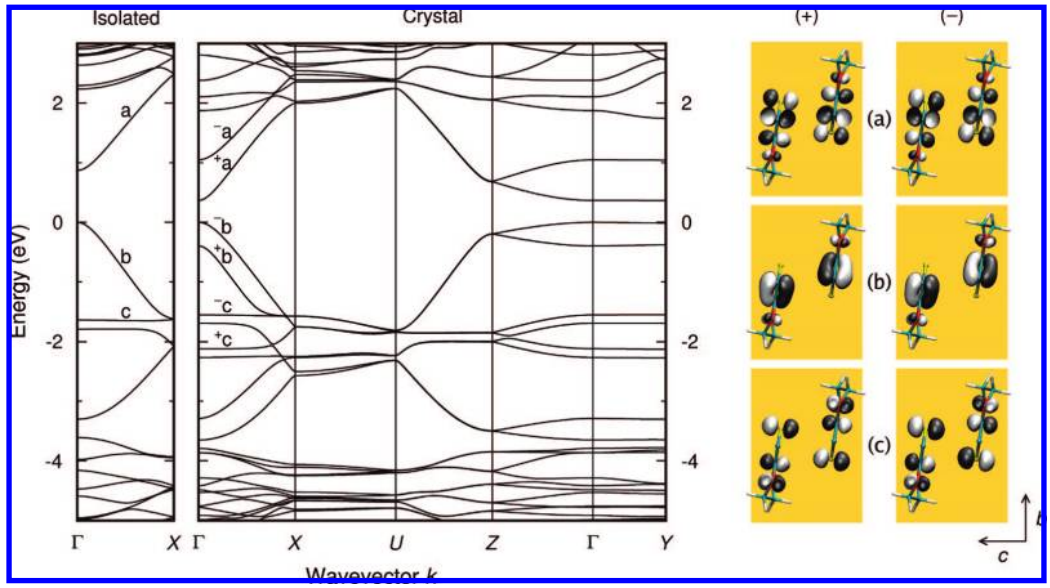

Figure 6. Electronic band structure of the pristine PEDOT crystal. The band structure of the isolated chain is also shown for comparison. The *k*-points of high symmetry in the first Brillouin zone of the orthorhombic lattice are labeled as follows: $X = (0.5, 0, 0)$; $Y = (0, 0.5, 0)$; $Z = (0, 0, 0.5)$; and $U = (0.5, 0, 0.5)$, all in crystallographic coordinates. The energy levels are shifted such that the valence band edge aligns with zero. To the right of the band structure panel are the wavefunction patterns, viewed down the *a*-axis, of the labeled subbands at Γ. Only the contents in the top half of the unit cell along the *a*-axis are shown for clarity.

geometry of the molecules within the unit cell, but also their pressure-dependent molecular orientations[61] and intra- and intermolecular vibrational properties,[62,63] in a variety of conjugated organic crystals where subtle $\pi-\pi$ interactions are at work. We note that the cell optimization performed with respect to the edge length *a* does not suffer from the issue discussed above because intramolecular bonding is dominant in this direction (parallel to the chain axis) and thus the role of van der Waals interactions is minimal.

Once the molecular packing is set, it is the wavefunction overlap that dictates electronic coupling. Recent experimental determinations of the intra- and intermolecular band structure of sexiphenyl via angle-resolved photoelectron spectroscopy[64] and of the hole effective mass in rubrene via infrared spectroscopy[65] further corroborate the validity of the use of DFT and GGA functionals for a theoretical description of both geometric and electronic structures of π-conjugated organic crystals.

3.2.2. Effects of Interchain Interactions on the Electronic Structure. Figure 6 shows the electronic band structure of the pristine crystal. We plotted the bands for the orthorhombic (instead of monoclinic) lattice, which will later allow for a direct comparison with the doped crystal. Two obvious consequences of the interchain interactions are the increased bandwidths and reduced bandgap (compare, for instance, the band structure along the backbone axis (Γ*X*) to that of the isolated chain; see also Table 2). The intrastack interactions along the *c*-axis, as indicated by the subband splitting in the Γ*Z* zone, are responsible for these changes; the interstack interactions along the *b*-axis are not, as indicated by the flat subbands in the Γ*Y* zone.

Comparison of the top two valence subbands and bottom two conduction subbands in the Γ*Z* zone indicates that the electronic coupling in the π-stacking direction is 1.7 times as strong for the LUMO level as for the HOMO level (the transfer integrals *t* estimated from a one-dimensional tight binding model are 170 and 99 meV for electrons and holes, respectively); the subband splitting can also be seen in Γ*X*. This difference is due to the presence of nodes on the sulfur atoms in the HOMO wavefunction, which results in a more limited interchain wavefunction overlap (see Figures 3 and 6 for the wavefunction patterns). The flat subbands of the isolated chain, having additional charge density on the sulfur atoms, undergo stronger interchain interactions in the crystal (see the subband c split into subbands $^{\pm}$c in Γ*X* or Γ*Z*).

The different degrees of subband splitting are also manifested in the effective mass along the *c*-axis, which is much lighter for the electron ($1.6m_0$) than for the hole ($4.8m_0$) (see Table 2). Interestingly, the hole effective mass in the *intermolecular* direction is quite large; reported values of the hole effective mass for typical organic crystals with high hole mobilities such as pentacene,[66] rubrene,[65] and pentathienoacene[67] are smaller than ∼2.

The introduction of interchain interactions, having increased the intrachain bandwidth, would bring down the intrachain effective mass, as is seen for the electron (see Table 2). However, this is not the case for the hole; together with the interchain effective mass results, the hole becomes heavier than the electron in the crystal (in all crystallographic directions).

3.3. Heavily Doped Crystal. The initial guess structure of the PEDOT:Tos crystal was constructed from the X-ray diffraction data of Aasmundtveit et al.[24] Their study revealed that the lamellar structure of the pristine PEDOT crystal is retained and that the Tos ions, in the form of monolayers, come in between the adjacent PEDOT stacks (see Figure 7 for the calculated crystal structure). The experimental unit cell (which corresponds to half the calculated unit cell; see below) contains four EDOT

(61) Hummer, K.; Puschnig, P.; Ambrosch-Draxl, C. *Phys. Rev. B* **2003**, *67*, 184105.
(62) Hermet, P.; Bantignies, J.-L.; Rahmani, A.; Sauvajol, J.-L.; Johnson, M. R.; Serein, F. *J. Phys. Chem. A* **2005**, *109*, 1684–1691.
(63) Kearley, G. J.; Johnson, M. R.; Tomkinson, J. *J. Chem. Phys.* **2006**, *124*, 044514.
(64) Koller, G.; Berkebile, S.; Oehzelt, M.; Puschnig, P.; Ambrosch-Draxl, C.; Netzer, F. P.; Ramsey, M. G. *Science* **2007**, *317*, 351–355.
(65) Li, Z. Q.; Podzorov, V.; Sai, N.; Martin, M. C.; Gershenson, M. E.; Di Ventra, M.; Basov, D. N. *Phys. Rev. Lett.* **2007**, *99*, 016403.

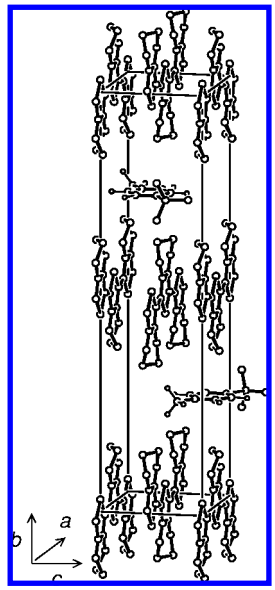

Figure 7. Calculated structure of the PEDOT:Tos crystal. The orthorhombic unit cell contains eight EDOT units from four chains and two Tos ions, with $b = 28.0$ Å and $c = 6.8$ Å from X-ray diffraction[24] and $a = 7.9$ Å calculated in this work. For clarity, hydrogen atoms on PEDOT and periodic images of Tos are not shown.

units from two polymer chains and one Tos ion, which is consistent with the doping level determined by XPS.[68]

The orientation of the Tos ions within the dopant layer, for which no experimental data are available, was determined in the course of our calculations. In order to accommodate the Tos ions between two adjacent PEDOT layers in an energetically favorable manner, it was found necessary that one PEDOT layer be symmetric with the other through a mirror plane embedded in the Tos layer, which in turn required twice the experimental unit cell size in the direction perpendicular to the layers (along the *b*-axis). The cell lengths *b*/2 and *c* were taken directly from experiment,[24] and *a* was optimized.

3.3.1. Tosylate Orientation and Interchain Geometry. It is useful to try and find the most favorable orientation for the Tos ions between two adjacent PEDOT layers, as a straightforward geometric consideration of the two strong driving forces, both of steric origin, would suggest. First, the Tos ion is too long to align parallel to the chain axis (the full molecular length between the two most distant C and S atoms is ~6.14 Å, which exceeds cell length *a*). Second, the bulky CH_3 and SO_3 groups can only be accommodated by a pair of two neighboring hollow sites sitting diagonally on the surface of each PEDOT layer (see Figure 8, right panel). With the Tos−PEDOT registration, it becomes obvious that the crystal structure of pristine PEDOT cannot accommodate the incoming Tos layers, because adjacent PEDOT layers have to be positioned in such a way that the intervening Tos layer serves as a mirror plane. In this puckered initial guess structure for the PEDOT layers, eight distinct ways of orienting two Tos ions in the unit cell are possible.

The most favorable crystal structure obtained after standard geometry optimization is shown in Figures 7 and 8. The space group determined from our calculations is $Pmn2_1$ in the standard orientation (where the unit cell is rotated by 90° around the *c*-axis). The long molecular axis of the Tos ions is 33.2° off the PEDOT chain axis within the dopant layer.

Doping-induced interchain geometric changes are quite significant; the chain rotation has vanished (<0.2°) and the PEDOT layers form a zigzag pattern along the *c*-axis (see Figure 8, left panel). A reduction in chain rotation was reported experimentally for iodine-doped P3ATs.[59] The zigzags within the PEDOT layer are due to the size difference between the

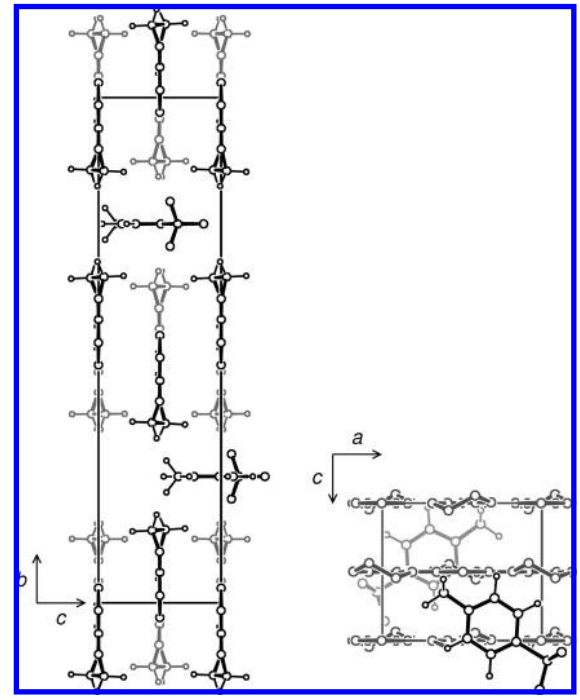

Figure 8. Registered structure of the calculated PEDOT:Tos crystal.

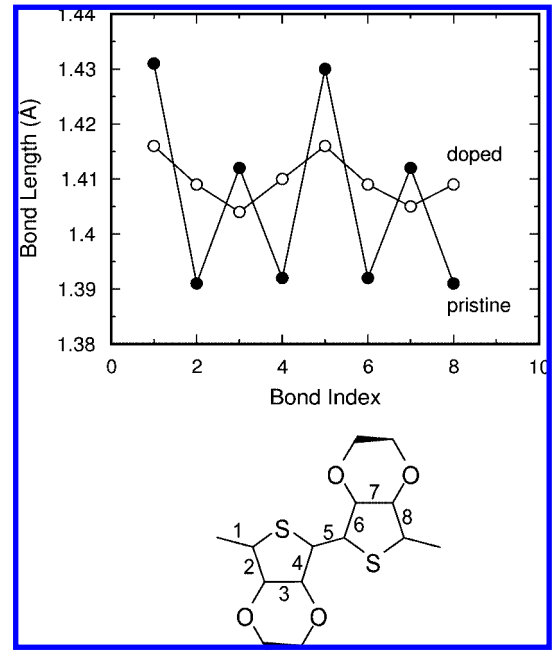

Figure 9. Effect of doping on the bond lengths along the chain backbone in the PEDOT:Tos crystal. Bonds 2−4 are close to SO_3 and bonds 6−8 are to CH_3. The bond lengths in the pristine crystal are also shown for comparison.

(66) de Wijs, G. A.; Mattheus, C. C.; de Groot, R. A.; Palstra, T. T. M. *Synth. Met.* **2003**, *139*, 109–114.
(67) Kim, E.-G.; Coropceanu, V.; Gruhn, N. E.; Sánchez-Carrera, R. S.; Snoeberger, R.; Matzger, A. J.; Brédas, J.-L. *J. Am. Chem. Soc.* **2007**, *129*, 13072–13081.
(68) Zotti, G.; Zecchin, S.; Schiavon, G.; Louwet, F.; Groenendaal, L.; Crispin, X.; Osikowicz, W.; Salaneck, W.; Fahlman, M. *Macromolecules* **2003**, *36*, 3337–3344.

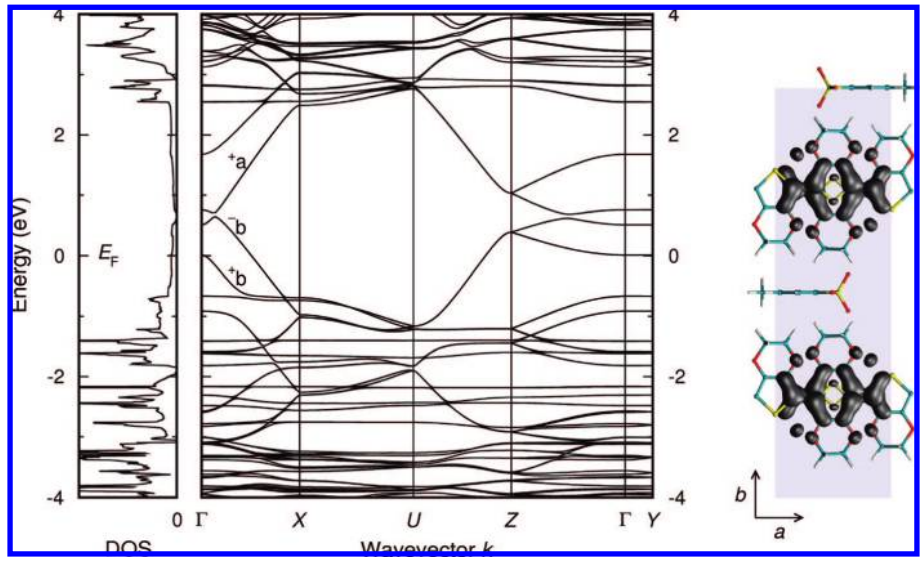

Figure 10. Band structure and the DOS of the PEDOT:Tos crystal. The high symmetry *k*-points in the first Brillouin zone are labeled as in Figure 6 for the pristine crystal. The energy levels are shifted such that the Fermi level E_F aligns with zero. Portions of the high intensity peaks in DOS are truncated in order to highlight the low intensity peaks. To the right of the plots is an illustration of the charge density at E_F.

CH_3 and SO_3 groups of the Tos ions, and explain why other configurations with both SO_3 groups in the same "column" along the *b*-axis are energetically unfavorable.

3.3.2. Doping-Induced Intrachain Geometry. Figure 9 shows the bond length alternation in the doped PEDOT crystal in comparison to the pristine crystal. Doping, as expected, leads to lengthening of the C=C bonds and shortening of the C−C bonds in the chain backbone. The new geometry can be best described as semiquinoid because the inter-ring bonds remain slightly larger than any other bonds. The calculated geometry shows that the oxidation shortens the chain length slightly (by 0.4%); an axial contraction was also observed experimentally in iodine-doped P3ATs.[59] The doping also causes geometric changes in the ethylenedioxy group; the C−O bonds shorten and the O−CH_2 bonds lengthen by about 0.02 Å, as a result of the oxygen atoms donating π-electrons to compensate the positive charges in the thiophene backbone.

3.3.3. Doping Effects on the Electronic Structure. The calculated band structure shows that the PEDOT:Tos crystal is metallic (see Figure 10). However, a close inspection indicates that this is the case only within the PEDOT layers; indeed, the flat subbands at the Fermi level in the Γ*Y* zone (along the *b*-axis) underline that this crystal is not conducting in the direction perpendicular to the PEDOT layers (see the right panel of Figure 10 for the nodal planes in charge density at the Tos layers at the Fermi level). The metallic nature and orientational anisotropy of PEDOT:Tos are in accord with optical reflectance and spectroscopic ellipsometry measurements[69,70] and are consistent with the significant electrical conductivity[7] (compare ∼1200 S/cm with <10 S/cm for PEDOT:PSS[4,71]).

All bands originating from the pristine PEDOT crystal keep very much their shape after doping; the valence bands, for instance, can easily be traced back if one removes the six (nearly) flat overlaid subbands in the energy range of −1.4 to −2.8 eV. These additional subbands involve mostly the Tos ions and give rise to the strongest peaks in the density of states (see Figure 10, left panel). Due to the very weak interactions along the *b*-axis as evident from the flatness in the Γ*Y* zone, all the subbands shown in Figure 10 are (quasi)degenerate (we recall that there are four PEDOT chains and two Tos ions in the unit cell of PEDOT:Tos).

The doping affects both intra- and interchain bandwidths, more prominently for the latter. A contraction by over 10% of the unit cell along the *c*-axis is responsible for the increase in bandwidth (compare the subband splitting in Γ*Z* between Figures 6 and 10).

3.3.4. Simulated UPS Spectrum of PEDOT:PSS. One of the goals of this study is to develop a reasonable theoretical model of PEDOT:PSS, which is a multiphase amorphous polymer blend. We show here that a two-phase model, based on PSSH representing the surface and PEDOT:Tos representing the bulk, can reproduce very well the electronic structure of PEDOT:PSS, as mapped by UPS.

Neutron reflectometry[13] and UPS[12] studies have confirmed that the surface of PEDOT:PSS films is covered with a thin layer of PSSH. In our calculations, PSSH was replaced by DSSH; PSSH being a large-gap insulator, its electronic structure does not depend significantly on chain length and tacticity.[72] The simulated UPS spectrum of PSSH, obtained by a standard procedure (see the Methodology section), is in excellent agreement with the experimental spectrum of the PEDOT:PSS surface, as shown in Figure 11, top panel. The slight offsets in intensity and location of the first peak are expected because of its sensitivity to water.[73]

For the bulk region of PEDOT:PSS, where the complex of positively charged PEDOT and segments of the PSSH chains that have lost protons exists in granular form with only the interstitial regions filled by PSSH,[15] we used the PEDOT:Tos crystal. This substitution is reasonable in that the doping level of PEDOT:PSS, independent of polymerization method and composition, is close to that of PEDOT:Tos (0.35 vs 0.25 in the number ratio of sulfur in sulfonate and thiophene).[68] We note that the contribution from the interstitial or shell PSSH is not accounted for in our model. Using the same simulation parameters as for the surface, we

(69) Pettersson, L. A. A.; Carlsson, F.; Inganäs, O.; Arwin, H. *Thin Solid Films* **1998**, *313−314*, 356–361.
(70) Pettersson, L. A. A.; Johansson, T.; Carlsson, F.; Arwin, H.; Inganäs, O. *Synth. Met.* **1999**, *101*, 198–199.
(71) Kirchmeyer, S.; Reuter, K. *J. Mater. Chem.* **2005**, *15*, 2077–2088.

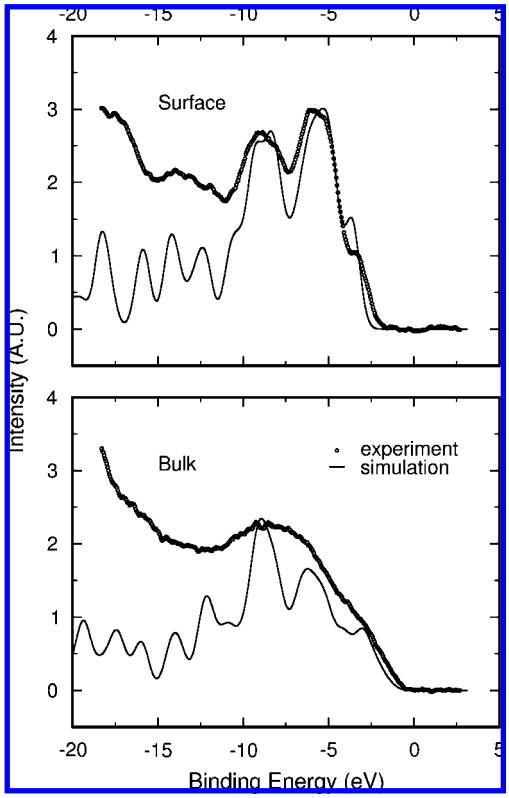

Figure 11. Simulated UPS spectra of PEDOT:PSS. The PSSH-rich surface region (top panel) is modeled by a single DSSH molecule, and the underlying bulk region (bottom panel) by the PEDOT:Tos crystal. The energy axes are scaled by a factor of 1.2. Experimental spectra from the work of Hwang et al.[12] are reproduced for comparison.

can successfully reproduce the main spectroscopic features of the electronic structure of PEDOT:PSS in the bulk, as shown in Figure 11, bottom panel. A single featureless experimental peak vs multiple simulated peaks reflects that PEDOT:PSS is mostly amorphous.[14] The underestimated intensities, especially in the high binding energy window, are due partly to the missing backbone bonds of PSS in Tos.

4. Conclusions

Using DFT methods, combined with an extensive analysis of crystallographic data, we have developed the first comprehensive three-dimensional model for the geometric and electronic structures of PEDOT in the pristine and doped states. The main results can be summarized as follows:

(1) PEDOT presents an aromatic-like geometry. Intrachain O···S binding between adjacent monomeric units, estimated to be on the order of 2.4 kcal/mol in energy, planarizes the chain backbone. The bandgap reduction with respect to PT is caused mostly by a stronger destabilization of the HOMO than the LUMO via donor-type substitution, rather than by planarization. The ethylenedioxy substitution reduces the intrachain charge carrier effective masses.

(2) The calculated crystal of pristine PEDOT adopts a monoclinic lamellar structure (space group $P2/c$). Within each π-stack, the chain backbones are rotated around the chain axis by $\sim 9°$. Interchain electronic coupling is almost twice as strong for the conduction band ($t = 170$ meV) as for the valence band ($t = 99$ meV). The intermolecular effective mass is $4.8m_0$ for holes and $1.6m_0$ for electrons; the latter is comparable to those for holes ($<2m_0$) in organic crystals with high charge carrier mobilities. As a result of interchain interactions, the *intrachain* effective mass decreases for electrons but *increases* for holes. In contrast to the isolated chain, the electrons are the lighter charge carrier in the pristine crystal (in all directions).

(3) The PEDOT:Tos crystal is found to have twice the unit cell size of the experimentally proposed structure. The unit cell proposed in the present work (space group $Pmn2_1$) carries a mirror plane between adjacent PEDOT stacks. The Tos molecules, sandwiched in a monolayer between PEDOT stacks, are locked in 33° off the chain axis, and cause the individual stacks to zigzag. Doping removes the chain backbone rotation found in the pristine crystal. The semiquinoid intrachain configuration keeps the inter-ring C−C bonds the longest. PEDOT:Tos is calculated to be a true metal within the PEDOT stacks but an insulator in the perpendicular direction. Doping increases the interchain bandwidth more prominently than the intrachain bandwidth. The simulation of recent UPS spectra indicates that a two-phase model based on PEDOT:Tos for the bulk and DSSH for the surface is able to represent PEDOT:PSS very well.

The present study of PEDOT:Tos appears to be especially timely following the recent use[7] of this doped form in replacement of ITO; PEDOT:Tos has been demonstrated as a patternable organic anode material in highly efficient OLEDs, where the need for organic alternatives to ITO is ever increasing. The structural model of PEDOT:Tos that has been developed here can be extended further to construct a model surface for studies of interfaces with organic semiconductors and related energy level alignments. Understanding of these interfaces is crucial to optimize the injection barrier, a key parameter in organic optoelectronic devices. Preliminary results show that such model surfaces can reproduce the experimental workfunction very well. We believe that the findings of our study also bring new insight into the control, via chemical modifications, over the bandgap and charge transport parameters in the polythiophene family.

Acknowledgment. We thank Prof. Antoine Kahn and Dr. Jaehyung Hwang at Princeton University for providing the original UPS data of PEDOT:PSS and for stimulating discussions, and Prof. Emil J. Samuelsen at Norges Teknisk-Naturvitenskapelige Universitet, Norway for the model crystal structure of PEDOT:Tos. We also thank Dr. Axel Kohlmeyer at the University of Pennsylvania for help with the CPMD code. Primary funding for this work by the Department of Energy (Award No. DE-FG02-04ER46165) is gratefully acknowledged. This work was also funded in part by the Office of Naval Research and by the National Science Foundation (CRIF Award No. CHE-0443564).

Supporting Information Available: Molecular coordinates of the calculated crystal structures of pristine PEDOT and PEDOT:Tos in CIF format and molecular coordinates and energies of T, EDOT, and their oligomers. This material is available free of charge via the Internet at http://pubs.acs.org.

JA806389B

(72) Ortí, E.; Brédas, J.-L.; Pireaux, J. J.; Ishihara, N. *J. Electron Spectrosc. Relat. Phenom.* **1990**, *52*, 551–570.
(73) Koch, N.; Vollmer, A.; Elschner, A. *Appl. Phys. Lett.* **2007**, *90*, 043512.